# Spectroscopic Characterization of a Reactive [Cu₂(μ-OH)₂]²⁺ Intermediate in Cu/TEMPO Catalyzed Aerobic Alcohol Oxidation Reaction

*Katrin Warm, Guilherme Tripodi, Erik Andris, Stefan Mebs, Uwe Kuhlmann, Holger Dau, Peter Hildebrandt, Jana Roithová,\* and Kallol Ray\**

**Abstract:** *Cuᴵ/TEMPO (TEMPO = 2,2,6,6-tetramethylpiperi-dinyloxyl) catalyst systems are versatile catalysts for aerobic alcohol oxidation reactions to selectively yield aldehydes. However, several aspects of the mechanism are yet unresolved, mainly because of the lack of identification of any reactive intermediates. Herein, we report the synthesis and character-ization of a dinuclear [**L1**₂Cu₂]²⁺ complex **1**, which in presence of TEMPO can couple the catalytic 4 H⁺/4 e⁻ reduction of O₂ to water to the oxidation of benzylic and aliphatic alcohols. The mechanisms of the O₂-reduction and alcohol oxidation reac-tions have been clarified by the spectroscopic detection of the reactive intermediates in the gas and condensed phases, as well as by kinetic studies on each step in the catalytic cycles. Bis(μ-oxo)dicopper(III) (**2**) and bis(μ-hydroxo)dicopper(II) species **3** are shown as viable reactants in oxidation catalysis. The present study provides deep mechanistic insight into the aerobic oxidation of alcohols that should serve as a valuable foundation for ongoing efforts dedicated towards the under-standing of transition-metal catalysts involving redox-active organic cocatalysts.*

## Introduction

Copper-oxygen species are proposed as reactive inter-mediates in a variety of biological and chemical oxidation reactions.[1] A significant effort has been dedicated towards the understanding of their electronic structures and reactiv-ities, which is necessary for obtaining detailed mechanistic insights into oxidation catalysis and for developing new, selective catalytic reagents and processes.[1b,c,2] In the last few decades, several reactive copper-oxygen motifs, exemplified by the structures **A**–**G** in Scheme 1, have been identified and
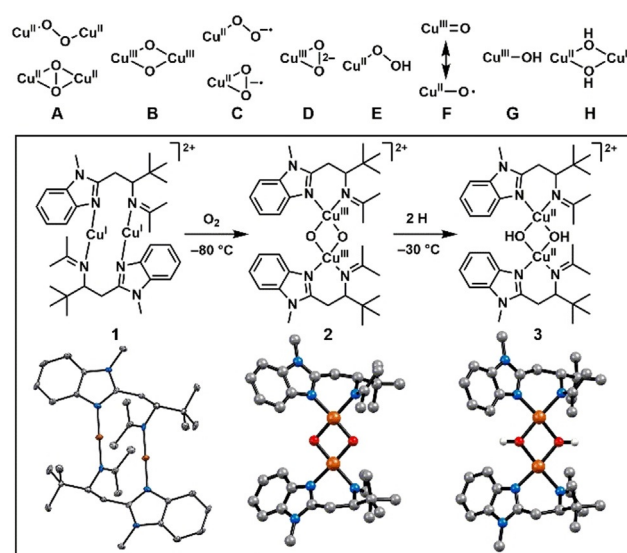


**Scheme 1.** Structures of the copper oxygen cores **A**–**H** and the dinuclear copper complexes **1**–**3** (**1**—XRD structure, **2**,**3**—DFT calcu-lated structures; Cu: orange, N: blue, C: grey, H: white).

spectroscopically characterized in the catalytic cycles of different copper containing enzymes and their synthetic model complexes.[1,3] We now report the generation and spectroscopic characterization of a new copper-oxygen inter-mediate **3** containing a bis(μ-hydroxo)dicopper(II) core (**H**), which is formed upon dioxygen activation at a dinuclear [**L1**₂Cu₂]²⁺ complex **1** (Scheme 1; **L1** = 3,3-dimethyl-1-(1-methyl-1*H*-benzo[*d*]imidazol-2-yl)-*N*-(propan-2-ylidene)bu-tan-2-amine). Furthermore, in contrast to previous reports, in

[*] M. Sc. K. Warm, Prof. Dr. K. Ray
Institut für Chemie, Humboldt-Universität zu Berlin
Brook-Taylor-Straße 2, 12489 Berlin (Germany)
E-mail: kallol.ray@chemie.hu-berlin.de

M. Sc. G. Tripodi, Dr. E. Andris, Prof. Dr. J. Roithová
Radboud University
Heyendaalseweg 135, 6525 AJ Nijmegen (Netherlands)
E-mail: j.roithova@science.ru.nl

Dr. E. Andris
Present Address Institute of Organic Chemistry and Biochemistry,
Czech Academy of SciencesFlemingovo náměstí 2, 16610 Prague
(Czech Republic)

Dr. S. Mebs, Prof. Dr. H. Dau
Institut für Physik, Freie Universität Berlin
Arnimallee 14, 14195 Berlin (Germany)

Dr. U. Kuhlmann, Prof. Dr. P. Hildebrandt
Institut für Chemie, Fakultät II, Technische Universität Berlin
Straße des 17. Juni 135, 10623 Berlin (Germany)

which copper(II)-hydroxide moieties are considered as sluggish oxidants in stoichiometric reactions[4] and products of catalyst decomposition reactions in Cu/TEMPO catalyzed aerobic oxidation of alcohols,[5] **3** is involved in the reduction of dioxygen to water in presence of 2,2,6,6-tetramethylpiperidin-1-ol (TEMPO-H) and also dehydrogenates aliphatic and benzyl alcohols in presence of the 2,2,6,6-tetramethylpiperidinyloxyl (TEMPO) radical. The unique reactivity of **3** makes the **1**/TEMPO system suitable for the catalytic aerobic oxidation of alcohols to aldehydes, by consuming all four oxidizing equivalents of $O_2$ and yielding $H_2O$ as a byproduct.

Notably, combinations of a $Cu^I$ salt and organic aminoxyl, such as TEMPO represent some of the most versatile and practical catalysts for the aerobic oxidation of alcohols to aldehydes.[5a,6] The most widely used catalysts feature 2,2′-bipyridine (bpy) as the ancillary ligand in combination with N-methyl imidazole (NMI). Replacement of bpy with a pyridine-imidazole (Py-NMI) ligand (2-(1-Methyl-1$H$-imidazol-2-yl)pyridine)[6d] in the above reaction has yielded comparable yields of the aldehyde product. However, several aspects of the mechanism remain unresolved and future studies are warranted to gain further insights that can guide the development of new catalytic systems. For example, although a mononuclear $[(bpy)Cu^I(NMI)]^+$ complex is proposed as an active catalyst responsible for dioxygen activation, this complex is generated in situ and has not been isolated and/or characterized. Furthermore, the isolation of a catalytically active tetranuclear $[(bpy)_4Cu_4(OH)_4](CF_3SO_3)_4$ cubane complex[5a] in the $Cu^I(OTf)$/bpy/NMI/TEMPO catalytic system makes the proposed bimolecular dioxygen activation mechanism ambiguous. Finally, a two electron reduction of $O_2$ to $H_2O_2$ (and its subsequent disproportionation to $H_2O$ and $O_2$) is proposed, in spite of the observed $O_2$:alcohol stoichiometry of 0.5[6b] that may point towards a direct four-electron reduction of $O_2$ to $H_2O$.

The growing synthetic utility and significance of the Cu/TEMPO catalyzed reactions and the existing mechanistic ambiguities prompted us to undertake a thorough mechanistic investigation. Based on the reported beneficial effect of imidazole ligation in copper catalyzed aerobic oxidation reactions in chemistry and biology,[1a,7] and the suggested bimolecular dioxygen activation mechanism[6b] in Cu/TEMPO catalyzed reactions, we now employ a well characterized dinuclear $[L1_2Cu^I_2]^{2+}$ complex **1** supported on a ligand **L1** bearing benzimidazole (Bzim) and imino (Imin) functionalities. Although **1**/NMI/TEMPO is slightly less efficient than $Cu^I(OTf)$/bpy/NMI/TEMPO (Table S1), the high level of steric hindrance provided by **L1** ensures successful trapping of some of the reactive intermediates formed upon dioxygen activation under catalytically relevant conditions. This study, therefore, provides a valuable foundation for ongoing efforts dedicated towards the understanding of transition-metal catalysts involving redox-active organic cocatalysts.[6c,8]

## Results and Discussion

The ligand **L1** bearing benzimidazole and imino functionalities was synthesized in a three-step reaction (Scheme S1).
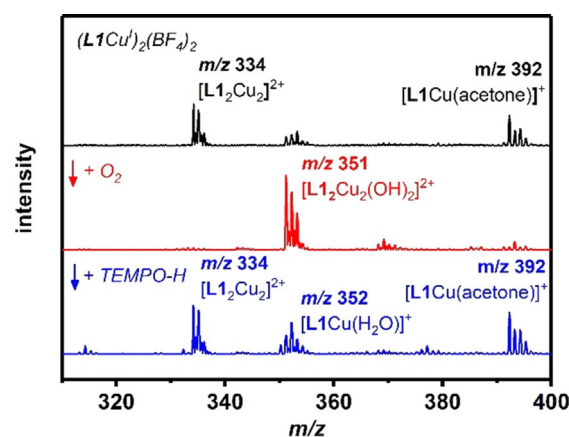


**Figure 1.** ESI-MS spectra of **1** in acetone in the positive mode displaying $[L1_2Cu_2]^{2+}$ ($m/z$ 334) and $[L1Cu(acetone)]^+$ ($m/z$ 392) (top, black); the reaction product of **1** with $O_2$ at −10°C displaying $[L1_2Cu_2(OH)_2]^{2+}$ (**3**) at $m/z$ 351 admixed with signals of $[L1Cu(OH)]^+$, $[L1_2Cu_2(OH)(F)]^{2+}$ and $([L1Cu(F)]^+$ (see Figure S5 for deconvolution) (middle, red); and the products of the addition of TEMPO-H to a solution of **3** corresponding to copper(I) complexes $[L1_2Cu_2]^{2+}$ ($m/z$ 334), $[L1Cu(H_2O)]^+$ ($m/z$ 352), and $[L1Cu(acetone)]^+$ ($m/z$ 392) (bottom, blue).

Metallation of **L1** with tetrakis(acetonitrile)copper(I) tetrafluoroborate yielded **1** in 63% yield. Electrospray ionization mass spectrometry (ESI-MS; Figure 1) of **1** shows a prominent signal of dimeric $[L1_2Cu_2]^{2+}$ at $m/z$ 334 and of monomeric $[L1Cu(acetone)]^+$ at $m/z$ 392.

Complex **1** is diamagnetic ($S = 0$), as demonstrated by the $^1H$ NMR resonances (Figure S2) spread over a chemical shift range of 0 to +10 ppm; the signals were shifted relative to the free ligand, thereby confirming the binding of $Cu^I$ to **L1**. X-ray diffraction (XRD) analysis revealed a dinuclear structure of **1** (Figure S3 and Scheme 1; Tables 1, S2), with **L1** acting as a bridging ligand between the two $Cu^I$ centers. The $Cu^I$ centers are two-coordinate with almost linear N-Cu-N angles of 176.55(19)° and $Cu-N^{Bzim}$ and $Cu-N^{Imin}$ distances of 1.877-(4) Å, and 1.903(4) Å, respectively. In X-ray absorption near-edge spectroscopic (XANES) studies at the Cu K-edge (Figure 2A), **1** exhibits an edge inflection energy of ≈8985.8 eV, with a shoulder along the rising edge at 8983.8 eV corresponding to a 1 s→4p shakedown transition, in accordance with the $Cu^I$ assignment and the linear

**Table 1:** Selected distances [Å] for complexes **1**, **2** and **3** as obtained from XRD and XAS measurements and DFT calculations.

| | | Cu—N$^{Bzim}$ | Cu—N$^{Imin}$ | Cu—O | Cu—Cu |
|---|---|---|---|---|---|
| **1** | XRD | 1.877(4) | 1.903(4) | – | 3.144(1) |
| | EXAFS | 1.91 | 1.91 | – | 3.19 |
| | DFT | 1.873 | 1.891 | – | 3.043 |
| **2** | EXAFS | 1.96 | 1.96 | 1.81 | 2.76 |
| | DFT | 1.890 | 1.946 | 1.780 1.786[a] | 2.715 |
| **3** | EXAFS | 1.96 | 1.96 | 1.96 | 3.01 |
| | DFT | 1.962 | 2.041 | 1.938 1.954[a] | 3.062 |

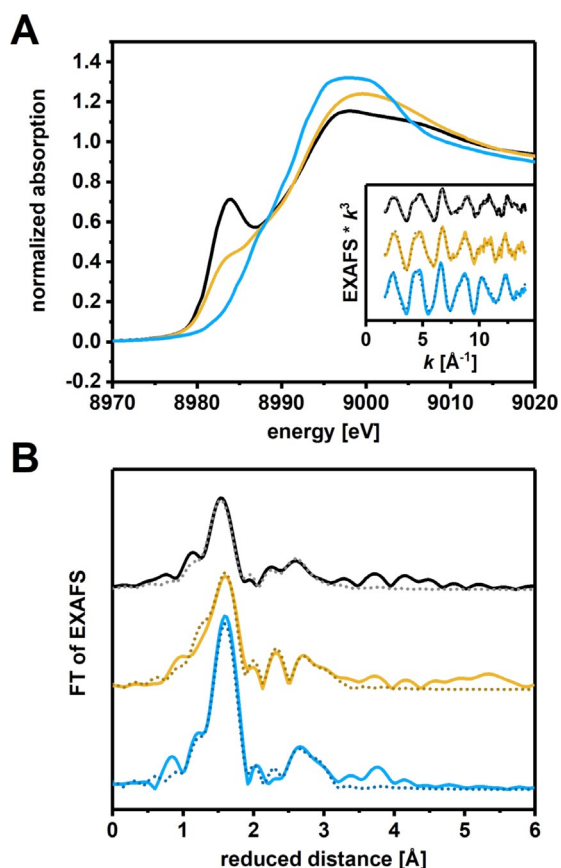[a] Asymmetric **L1** coordination to copper results in a distorted $Cu_2O_2$ core structure.

**Figure 2.** A) X-ray absorption near edge fine structure (XANES) spectra of solutions of **1** (black), **2** (yellow) and **3** (blue) in *[D₆]*acetone; extended X-ray absorption fine structure (EXAFS) data are shown as an inset (solid lines: experimental spectra, dotted lines: simulated spectra); B) Fourier transformation of the EXAFS signals of **1** (black), **2** (yellow) and **3** (blue); for further details concerning bond distances and simulation parameters see table S3.

coordination of Cu. Analysis of the extended X-ray absorption fine structure (EXAFS) spectra revealed 2 N scatterers at 1.91 Å and 1 Cu scatterer at 3.19 Å (Figure 2, Tables 1, S3). The good agreement between XRD and EXAFS determined
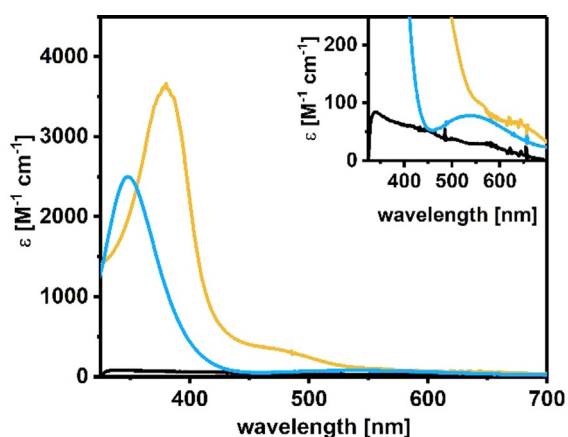


**Figure 3.** UV/Vis absorption spectra of **1** (black), **2** (yellow) and **3** (blue); the expansion of the 400–600 nm region is shown as an inset.

distances (Tables 1, S2, S3) confirms that the dinuclear solid-state structure is retained in frozen acetone solutions of **1**.

Complex **1** reacts with $O_2$ in acetone and acetonitrile at −30 °C to yield a new species **3** (Figure 3, $t_{1/2} \approx 5$ h @ 20 °C in acetone) with electronic absorption maxima centered at 345 nm ($\varepsilon_{max} = 2500$ M⁻¹ cm⁻¹) and at 540 nm ($\varepsilon_{max} = 80$ M⁻¹ cm⁻¹). The nature of **3** was established by a variety of spectroscopic techniques. Complex **3** is silent at X-band EPR (Figure S4). ESI-MS (Figure 1, red) shows a signal at $m/z$ 351 corresponding to dimeric $[\mathbf{L1}_2Cu_2(OH)_2]^{2+}$. The isotopic pattern suggests that we also detect monomeric $[\mathbf{L1}Cu(OH)]^+$ and $[\mathbf{L1}Cu(F)]^+$ and their dimer $[\mathbf{L1}_2Cu_2(OH)(F)]^{2+}$ (see Figure S5 for the deconvolution of the signals). Fluorine originates from decomposition of $BF_4^-$ counterions. Upon introduction of ¹⁸O into **3**, its mass shifts from 351.1 to 353.1 (Figure S6), thereby demonstrating that two oxygen atoms from ¹⁸$O_2$ are incorporated into the $[\mathbf{L1}_2Cu_2(OH)_2]^{2+}$ core in **3**. Upon addition of $D_2O$, we observe a shift towards formation of $[\mathbf{L1}_2Cu_2(OD)_2]^{2+}$ (Figure S6).

We have further investigated the structure of $[\mathbf{L1}_2Cu_2(OH)_2]^{2+}$ by helium tagging infrared photodissociation (IRPD) spectroscopy[9] (Figure 4 A). This method provides IR spectra of mass-selected ions (for more details see ref. [10]). The IR spectrum of gaseous $[\mathbf{L1}_2Cu_2(OH)_2]^{2+}$ reveals two oxygen-sensitive bands at 870 and 899 cm⁻¹, which shift to
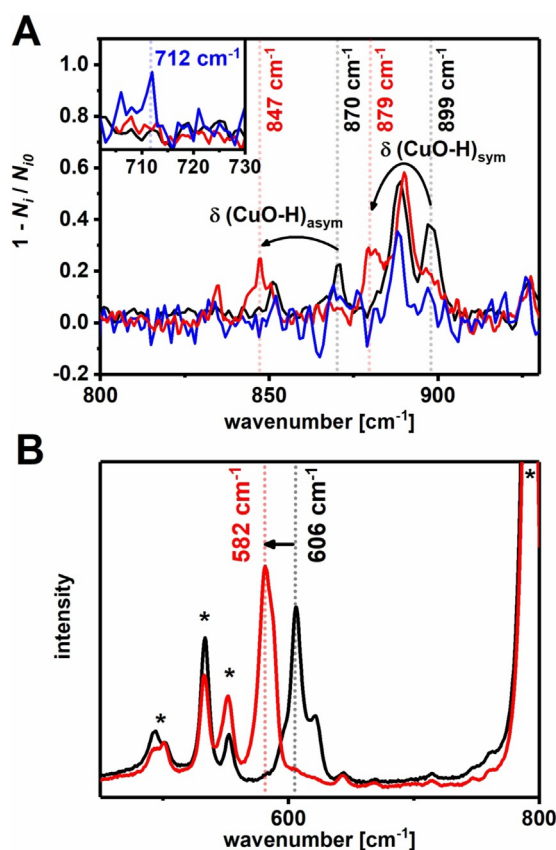


**Figure 4.** A) IR spectra of mass-selected ions of ¹⁶O-labelled **3** ($m/z$ 351.1, black), ¹⁸O-labelled **3** ($m/z$ 353.1, red) and ²H-labelled **3** ($m/z$ 352.1, blue) measured by helium-tagging IR photodissociation spectroscopy; the expansion of the 703-730 cm⁻¹ region is shows as an inset; B) rRaman spectra of ¹⁶O-labelled **2** (black) and ¹⁸O-labelled **2** (red) upon 406 nm Kr⁺ laser irradiation at −90 °C.

847 and 879 cm$^{-1}$, respectively, upon $^{18}$O-labelling. The $^1$H/$^2$H exchange in [**L1**$_2$Cu$_2$(OH)$_2$]$^{2+}$ results in a shift of the 899 cm$^{-1}$ band to 712 cm$^{-1}$; the 870 cm$^{-1}$ band also disappears upon $^1$H/$^2$H exchange, and is presumably shifted below 700 cm$^{-1}$, which is beyond the detection range of our spectrometer.

XANES of **3** in acetone provides an edge-energy of 8987.1 eV, which is blue-shifted relative to **1**, and consistent with a Cu$^{II}$ assignment (Figure 2A). Analysis (Figure 2; Tables 1, S3) of the EXAFS spectrum shows 4 Cu-N/O and 1 Cu-Cu shells at 1.96 Å and 3.01 Å, respectively, for **3**, which are in the range of the Cu-N/O and Cu-Cu distances observed in the crystallographically characterized [Cu$_2$(OH)$_2$]$^{2+}$ cores in the literature (Table S4).[4a,c,d,f,g]

Taken together, all the spectroscopic studies point towards a bis(μ-hydroxo)dicopper(II) assignment for **3**, which is also supported by density functional theoretical studies. The lowest energy structure corresponds to a [**L1**Cu$^{II}$(μ-OH)$_2$Cu$^{II}$**L1**]$^{2+}$ motif, where antiferromagnetic coupling between the $S_{Cu} = 1/2$ Cu$^{II}$ centers stabilizes an open-shell $S_T = 0$ electronic configuration (Scheme 1; Figure S7). The most stable isomers **A** and **B** differ by the benzimidazole units pointing the same or to opposite sides of the dicopper complex. The energies of the isomers lie within 1 kcal mol$^{-1}$. Each of the isomers can also have other conformers (e.g., **C** in Figure S7). The positions of the IR-active bands involving the Cu$^{II}$(μ-OH)$_2$Cu$^{II}$ core and their $^{18}$O/$^{16}$O and $^1$H/$^2$H isotopic shifts are in a reasonable agreement with the experimental values (Figure S7 and Tables 1, S6). On the basis of the calculated frequencies and isotopic shifts (Table S6), the experimentally observed IR bands at 877 ($^{18}$O/$^{16}$O shift of 23 cm$^{-1}$) and 899 cm$^{-1}$ ($^{18}$O/$^{16}$O and $^1$H/$^2$H shifts of 20 and 187 cm$^{-1}$, respectively) are assigned to symmetric and anti-symmetric CuO-H deformation modes. For instance, the calculated frequencies for isomer **B** are 866 cm$^{-1}$ and 878 cm$^{-1}$, with $^{18}$O/$^{16}$O shifts of 20 cm$^{-1}$ and 18 cm$^{-1}$, respectively. Upon $^2$H substitution the 878 cm$^{-1}$ mode is shifted to 690 cm$^{-1}$, in good agreement with the experiment. The experimentally observed Cu-N/O distances are also well reproduced in the calculations (Tables 1, S6).

The conversion of **1** to **3** in the presence of O$_2$ must involve the initial formation of a transient Cu-dioxygen intermediate, **2**, followed by a rapid H-atom abstraction (HAA) from acetone. Indeed, a comparison of the rates of the formation of **3** in acetone and *[D$_6$]acetone*, yields a hydrogen/deuterium kinetic isotope effect (KIE) of 1.65 (Figure S8, Table S7), which corroborates acetone as a H-atom donor in the reaction. Adjustment of the reaction conditions to ensure faster formation of **2** and its slower decay to **3**, led to the eventual trapping of **2**. Accordingly, the reaction of a concentrated solution of **1** (≥2.5 mM) with O$_2$ at −80°C in *[D$_6$]acetone* results in the development of an intense absorption feature at 375 nm ($\varepsilon_{max} = 3700$ M$^{-1}$ cm$^{-1}$) and a weaker band at 465 nm ($\varepsilon_{max} = 360$ M$^{-1}$ cm$^{-1}$) ($t_{1/2} = 10$ min at −30°C in *[D$_6$]acetone*) corresponding to **2** (Figure 3). In presence of substrates bearing weak O−H (e.g. TEMPO-H) or C−H bonds (e.g. 1,4-cyclohexadiene and indene) **2** is converted to **3**, with an isosbestic point at 356 nm (Figures 5A, S9–11, Table S8). This plausibly implies a single-step mechanism for the two HAA steps required for the conversion of **2** to **3**.
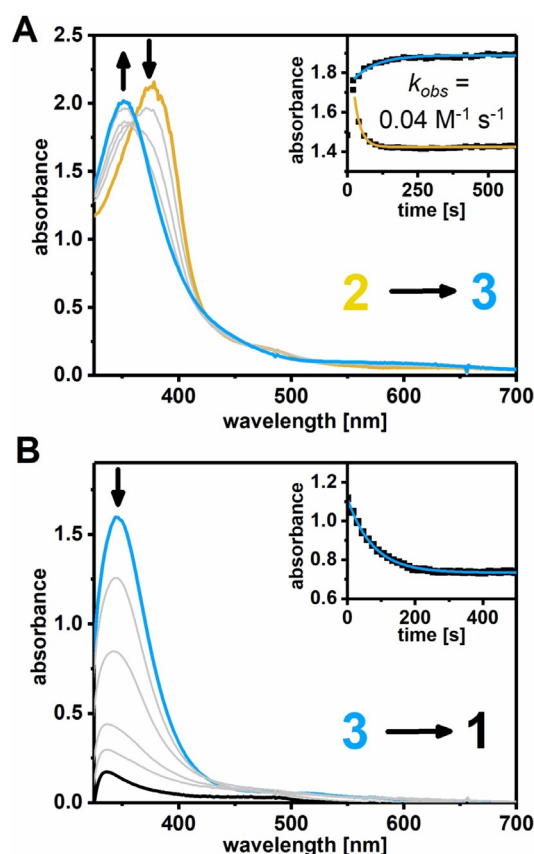


**Figure 5.** A) Changes in the UV/Vis spectra of **2** (yellow) and formation of 3 (blue) upon addition of 1,4-cyclohexadiene (0.07 M) at −90°C; inset shows the time traces at the characteristic wavelengths of **2** (375 nm, yellow first-order fit) and **3** (345 nm, blue first-order fit); B) Changes in the UV/Vis spectra of **3** (blue) upon addition of TEMPO-H (0.05 M) at −50°C yielding **1**; inset shows the time-trace at 345 nm.

Resonance Raman (rRaman) spectroscopy performed on solutions of **2** in acetone displays a ν(Cu-O) stretching vibration at 606 cm$^{-1}$, which shifts to 582 cm$^{-1}$ upon $^{18}$O-labelling (Figure 4B). XANES of **2** shows the presence of residual **1** in solution, which together with the lack of any pre-edge in **2** removes the one sure way of assigning the physical oxidation state of copper (Cu$^{II}$ vs Cu$^{III}$); edge energies are known to be an ambiguous predictor for identifying whether a given complex is Cu$^{II}$ or Cu$^{III}$.[11] EXAFS analysis of **2** reveals short Cu-O and Cu-Cu distances of 1.81 Å and 2.76 Å, respectively. In analogy to the well-studied [Cu$^{III}$$_2$(μ-O)$_2$]$^{2+}$ systems,[1b,8b,c] for which similar EXAFS, rRaman and absorption spectral signatures were reported, we assign **2** as a [**L1**Cu$^{III}$(μ-O)$_2$Cu$^{III}$**L1**] complex (Table S5). The DFT calculated ν([Cu-O]$_2$) and Cu-N/O and Cu-Cu distances are in reasonable agreement with the experiment (Tables 1, S6), further validating the [Cu$^{III}$$_2$(μ-O)$_2$]$^{2+}$ assignment of **2**. The HAA reactivity of **2** with 1,4-CHD is one order of magnitude slower than some of the most reactive [Cu$^{III}$$_2$(μ-O)$_2$]$^{2+}$ complexes known to date (Table S5).[1b,8b,c]

Based on the proposed involvement of transient [Cu$^{II}$-OH]$^+$ intermediates[6a–c] in the Cu/TEMPO catalyzed aerobic oxidation of alcohols, we sought to investigate the reactivity
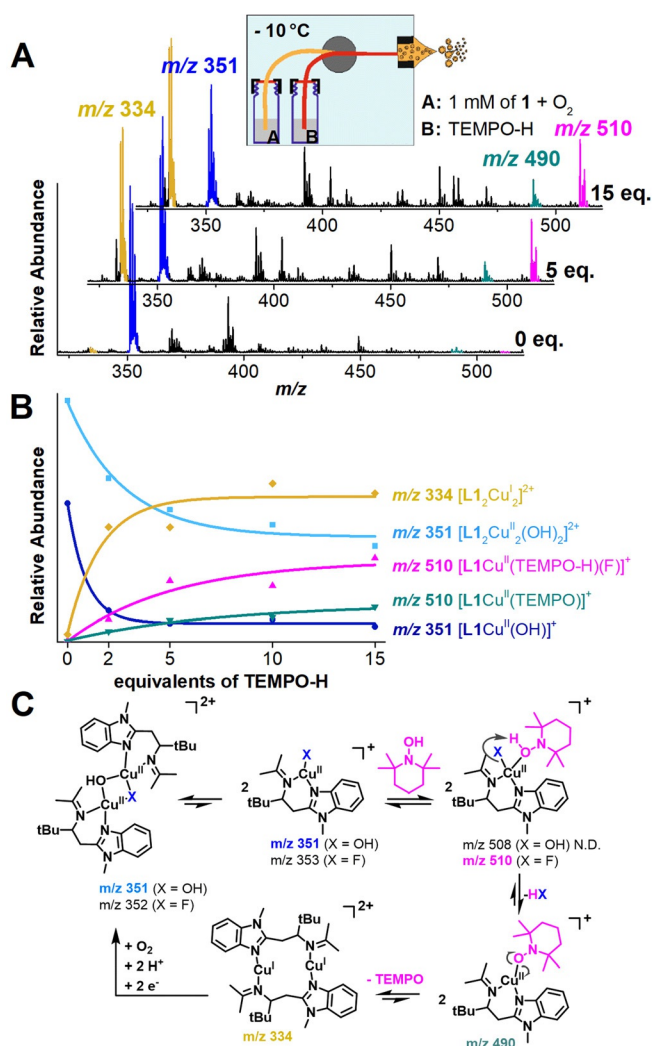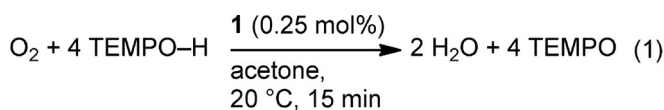
**Figure 6.** A) ESI-MS spectra at constant reaction time with varied concentrations of TEMPO-H (indicated at the right side); B) Relative integrated intensities of the signals corresponding to copper(II) reactants and copper(I) products; the corresponding ions are color-coded; C) The reaction Scheme consistent with the kinetics obtained from the flow reactor—ESI-MS experiments.

of the $[Cu_2(\mu\text{-}OH)_2]^{2+}$ core in **3** in various oxidation reactions. In HAA reaction, the addition of TEMPO-H to an acetone solution of **3** at 20°C leads to the decay of the 345 nm band corresponding to **3** with the stoichiometric formation of TEMPO (Figure 6B, Figure S12). The first-order rate constant, determined by pseudo-first-order fitting of the kinetic data for the decay of **3**, increases linearly with increasing TEMPO-H concentration, thereby giving a second-order rate constant of $0.12\ \text{M}^{-1}\text{s}^{-1}$ at $-50$°C (Figure S12).

We have further monitored the reaction of **3** and TEMPO-H by ESI-MS.[12] We have shortened the reaction time to the order of seconds by performing the reaction in a flow setup and studied the reaction kinetics by changing the concentration of TEMPO-H (Figure 6).[13] The spectra show an increasing conversion of the dimer **3** and $[\textbf{L1}Cu(OH)]^+$ to the copper(I) dimer **1** with the increasing concentration of TEMPO-H (Figure 6. blue to yellow, see also Figure S5)). The dependence of the relative ion abundances on the concen-
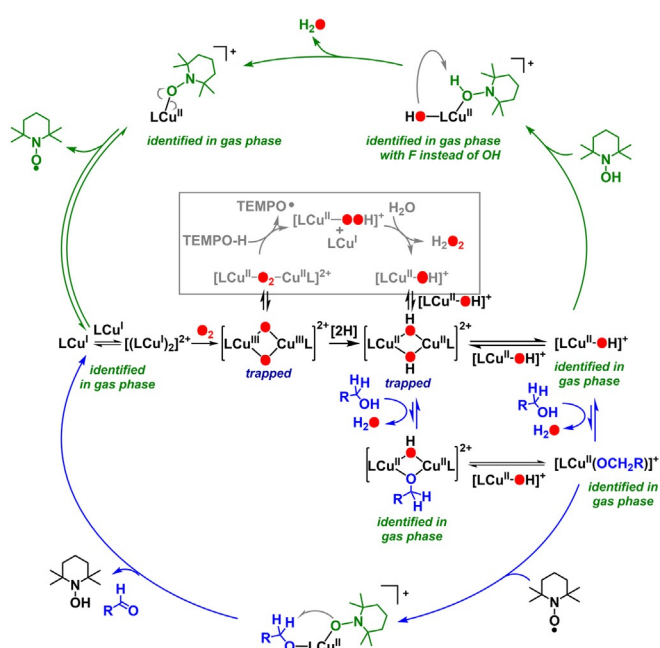
tration of TEMPO-H clearly suggests that the monomer $[\textbf{L1}Cu(OH)]^+$ reacts faster than the dimer (Figure 6B). In fact, the decreasing concentration of **3** is most likely a result of the equilibrium reaction between **3** and the $[\textbf{L1}Cu(OH)]^+$ monomer; however, a direct reaction of **3** with TEMPO-H can't be excluded. In addition, we detect intermediates of this transformation. The $[\textbf{L1}Cu(OH)]^+$ complex reacts with TEMPO-H to form $[\textbf{L1}Cu(OH)(TEMPOH)]^+$, which eliminates $H_2O$ and yields $[\textbf{L1}Cu(TEMPO)]^+$ (in green in Figure 6). This intermediate eliminates the TEMPO radical leading to the regeneration of the copper(I) complex. We did not detect the primary $[\textbf{L1}Cu(OH)(TEMPOH)]^+$ intermediate, but we did detect analogous $[\textbf{L1}Cu(F)(TEMPOH)]^+$ (in pink). This complex can be interpreted as a "frozen" intermediate, because the large electronegativity of F makes the elimination of HF endothermic (see also Figure S13), thereby leading to the accumulation of $[\textbf{L1}Cu(F)(TEMPOH)]^+$.

The direct cleavage of oxygen by **1** to form **3** and the subsequent regeneration of **1** from **3** in presence of a H-atom donor makes **1** an efficient catalyst for the reduction of $O_2$ to $H_2O$ without forming $H_2O_2$ as an intermediate or byproduct, which has tremendous technological significance.[14] In a test reaction, 0.25 mol% of **1** in acetone at 20°C was found to be able to catalytically reduce $O_2$ to $H_2O$ with a turn-over number (TON) of 250 by employing TEMPO-H as a H-atom donor [Eqn. (1); Figure S14].[15] The involvement of **2** and **3** could be evidenced by using the stopped-flow technique in the reaction of **1** and $O_2$ in presence of excess TEMPO-H at $-75$°C; at higher temperature the $Cu^I$ species is regenerated by the reaction of **3** with TEMPO-H (Figure S11).

$$O_2 + 4\ \text{TEMPO–H} \xrightarrow[\substack{\text{acetone,}\\20\ °C,\ 15\ \text{min}}]{\textbf{1}\ (0.25\ \text{mol}\%)} 2\ H_2O + 4\ \text{TEMPO} \quad (1)$$
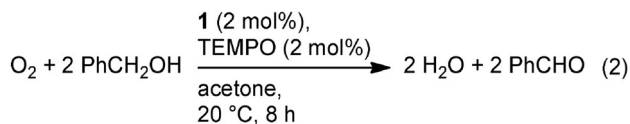
Complex **3** also showed a high reactivity in the oxidation of benzyl alcohol at 20°C in presence of TEMPO, thereby producing benzaldehyde quantitatively and regenerating **1** and TEMPO-H. Addition of 100 equiv of benzylalcohol to a solution of **3** leads to a red-shift of the 345 nm band to 355 nm (Figure S15), presumably because of the formation of the $[\textbf{L1}Cu^{II}(\mu\text{-}OCH_2Ph)(\mu\text{-}OH)Cu^{II}\textbf{L1}]$ (**4**) in a preequilibrium step (Scheme 2), as evident from ESI-MS (Figure S16) and EPR spectroscopy (Figure S17). Complex **4** then decays in presence of TEMPO with a second order rate constant of $0.05\ \text{M}^{-1}\text{s}^{-1}$ at $-10$°C (Figure S15). **3** can also dehydrogenate aliphatic alcohols like *n*-hexanol in presence of TEMPO to the corresponding aldehydes (30% yield), but at rates much slower than benzylalcohol (Figure S18).

Based on the demonstrated abilities of **3** to dehydrogenate benzylalcohol in presence of TEMPO and to regenerate TEMPO by HAA from TEMPO-H, we tested the aerobic oxidation of benzylalcohol under catalytic conditions [Eqn. (2)]. Indeed, in presence of $O_2$ or air in acetone at 20°C, **1** (2 mol%) and TEMPO (2 mol%) can catalytically oxidize benzyl alcohol to benzaldehyde with a moderate TON of 25;[15] however, our aliphatic model substrate *n*-hexanol

**Scheme 2.** Overview of the mechanisms of catalytic alcohol oxidation (blue) and O$_2$ reduction reactions (green); the inset shows the different O$_2$ activation mechanism suggested by Stahl et al.[6b]

was only oxidized to *n*-hexanal stoichiometrically. Interestingly, the addition of NMI (4 mol%) enabled the catalytic oxidation of *n*-hexanol (TON = 7) and also enhanced the catalytic efficiency of the oxidation of benzyl alcohol (TON ≥ 50).

$$O_2 + 2\ PhCH_2OH \xrightarrow[\substack{acetone, \\ 20\,°C,\ 8\ h}]{\substack{\textbf{1}\ (2\ mol\%), \\ TEMPO\ (2\ mol\%)}} 2\ H_2O + 2\ PhCHO \quad (2)$$

The effect of NMI addition on the reaction was evaluated under stoichiometric conditions. An instantaneous decay of the UV/Vis features of **3** upon addition of 5 equiv NMI at −10°C indicated a substantial structural change. This was corroborated by EPR, which showed the formation of a paramagnetic mononuclear Cu$^{II}$ species in 60% yield (Figure S19). Hence we conclude that NMI not only acts as a base, as suggested previously, thereby, assisting the formation of the Cu$^{II}$-alcoholate complex **4**,[5a,6a,b] it also presumably facilitates the dissociation of the [**L1**Cu$^{II}$(μ-OH)Cu$^{II}$**L1**]$^{2+}$ dimer into the more reactive [**L1**Cu(OH)]$^+$ monomer.

## Conclusion

In summary, bis(μ-oxo)dicopper(III) and bis(μ-hydroxo)dicopper(II) species have been identified and spectroscopically characterized as reactive intermediates in **1**/TEMPO catalyzed aerobic oxidation of benzylalcohol and *n*-hexanol. Our study supports a mechanism, in which the catalytic 4H$^+$/4e$^-$ reduction of O$_2$ to water is coupled to the

oxidation of alcohols (Scheme 2). Although the mechanism for **1**/TEMPO parallels the proposed bimolecular activation of O$_2$ during (bpy)Cu$^I$/TEMPO catalyzed aerobic oxidation of alcohols,[6b] the results of our study also reveal some differences in the two cases. For example, in the (bpy)Cu$^I$/TEMPO system, based on detailed kinetic studies, an unidentified transient binuclear Cu$_2$O$_2$ intermediate was proposed to convert to a mononuclear Cu$^{II}$-OH species (responsible for alcohol oxidation) in presence of TEMPO-H and H$_2$O with the release of H$_2$O$_2$ (Scheme 2, inset shown in grey). In contrast, the two Cu$^I$ centers in **1** are demonstrated to directly cleave O$_2$ to form a well characterized bis(μ-oxo)dicopper-(III) intermediate **2**, which undergoes HAA reactions to yield the bis(μ-hydroxo)dicopper(II) moiety **3**. Complex **3** reacts with TEMPO-H to release water, thereby forming TEMPO, which is then used in the dehydrogenation of alcohols. The direct cleavage of O$_2$ by **1** ensures the clean reduction of O$_2$ to H$_2$O without any formation of H$_2$O$_2$. Notably, the previous report[5a] of the precipitation of [(bpy)$_4$Cu$_4$(OH)$_4$](CF$_3$SO$_3$)$_4$ may also corroborate the involvement of a similar [(bpy)$_2$Cu$_2$-(OH)$_2$](CF$_3$SO$_3$)$_2$ core during the bpy/Cu$^I$/TEMPO/NMI catalyzed aerobic oxidation of alcohols; the lower steric demand of bpy plausibly makes [(bpy)$_2$Cu$_2$(OH)$_2$](CF$_3$SO$_3$)$_2$ unstable against dimerization leading to the precipitation of [(bpy)$_4$Cu$_4$(OH)$_4$](CF$_3$SO$_3$)$_4$.

## Acknowledgements

## Conflict of Interest

The authors declare no conflict of interest.

[1] a) E. I. Solomon, D. E. Heppner, E. M. Johnston, J. W. Ginsbach, J. Cirera, M. Qayyum, M. T. Kieber-Emmons, C. H. Kjaergaard, R. G. Hadt, L. Tian, *Chem. Rev.* **2014**, *114*, 3659–3853; b) C. E. Elwell, N. L. Gagnon, B. D. Neisen, D. Dhar, A. D. Spaeth, G. M. Yee, W. B. Tolman, *Chem. Rev.* **2017**, *117*, 2059–

2107; c) D. A. Quist, D. E. Diaz, J. J. Liu, K. D. Karlin, *J. Biol. Inorg. Chem.* **2017**, *22*, 253–288.

[2] R. Trammell, K. Rajabimoghadam, I. Garcia-Bosch, *Chem. Rev.* **2019**, *119*, 2954–3031.

[3] a) P. J. Donoghue, J. Tehranchi, C. J. Cramer, R. Sarangi, E. I. Solomon, W. B. Tolman, *J. Am. Chem. Soc.* **2011**, *133*, 17602–17605; b) N. Gagnon, W. B. Tolman, *Acc. Chem. Res.* **2015**, *48*, 2126–2131.

[4] a) S. Mahapatra, J. A. Halfen, E. C. Wilkinson, G. Pan, X. Wang, V. G. Young, C. J. Cramer, L. Que, W. B. Tolman, *J. Am. Chem. Soc.* **1996**, *118*, 11555–11574; b) E. Ruiz, P. Alemany, S. Alvarez, J. Cano, *J. Am. Chem. Soc.* **1997**, *119*, 1297–1303; c) H. V. Obias, Y. Lin, N. N. Murthy, E. Pidcock, E. I. Solomon, M. Ralle, N. J. Blackburn, Y.-M. Neuhold, A. D. Zuberbühler, K. D. Karlin, *J. Am. Chem. Soc.* **1998**, *120*, 12960–12961; d) R. Haase, T. Beschnitt, U. Flörke, S. Herres-Pawlis, *Inorg. Chim. Acta* **2011**, *374*, 546–557; e) M. R. Halvagar, P. V. Solntsev, H. Lim, B. Hedman, K. O. Hodgson, E. I. Solomon, C. J. Cramer, W. B. Tolman, *J. Am. Chem. Soc.* **2014**, *136*, 7269–7272; f) N. Kitajima, T. Koda, S. Hashimoto, T. Kitagawa, Y. Morooka, *J. Am. Chem. Soc.* **1991**, *113*, 5664–5671; g) S. Herres, U. Florke, G. Henkel, *Acta Crystallogr. Sect. C* **2004**, *60*, m659–m660.

[5] a) J. M. Hoover, B. L. Ryland, S. S. Stahl, *ACS Catal.* **2013**, *3*, 2599–2605; b) E. T. T. Kumpulainen, A. M. P. Koskinen, *Chem. Eur. J.* **2009**, *15*, 10901–10911.

[6] a) J. M. Hoover, S. S. Stahl, *J. Am. Chem. Soc.* **2011**, *133*, 16901–16910; b) J. M. Hoover, B. L. Ryland, S. S. Stahl, *J. Am. Chem. Soc.* **2013**, *135*, 2357–2367; c) B. L. Ryland, S. S. Stahl, *Angew. Chem. Int. Ed.* **2014**, *53*, 8824–8838; *Angew. Chem.* **2014**, *126*, 8968–8983; d) J. E. Steves, S. S. Stahl, *J. Am. Chem. Soc.* **2013**, *135*, 15742–15745; e) J. M. Hoover, J. E. Steves, S. S. Stahl, *Nat. Protoc.* **2012**, *7*, 1161–1166.

[7] a) M. Daou, C. B. Faulds, *World J. Microbiol. Biotechnol.* **2017**, *33*, 87; b) J. W. Whittaker, *Arch. Biochem. Biophys.* **2005**, *433*, 227–239.

[8] a) D. Wang, A. B. Weinstein, P. B. White, S. S. Stahl, *Chem. Rev.* **2018**, *118*, 2636–2679; b) C. Citek, S. Herres-Pawlis, T. D. P. Stack, *Acc. Chem. Res.* **2015**, *48*, 2424–2433; c) L. M. Mirica, X. Ottenwaelder, T. D. P. Stack, *Chem. Rev.* **2004**, *104*, 1013–1046.

[9] a) J. Roithová, A. Gray, E. Andris, J. Jašík, D. Gerlich, *Acc. Chem. Res.* **2016**, *49*, 223–230; b) D. Gerlich, *J. Chin. Chem. Soc.* **2018**, *65*, 637–653.

[10] For reviews about photodissociation spectroscopy see: a) L. Jašíková, J. Roithová, *Chem. Eur. J.* **2018**, *24*, 3374–3390; b) H. Schwarz, K. R. Asmis, *Chem. Eur. J.* **2019**, *25*, 2112–2126; c) P. Maitre, D. Scuderi, D. Corinti, B. Chiavarino, M. E. Crestoni, S. Fornarini, *Chem. Rev.* **2020**, *120*, 3261–3295. For the use of helium tagging IRPD spectroscopy for characterization of reactive metal complexes see: d) E. Andris, R. Navrátil, J. Jašík, M. Puri, M. Costas, L. Que, Jr., J. Roithová, *J. Am. Chem. Soc.* **2018**, *140*, 14391–14400; e) E. Andris, R. Navrátil, J. Jašík, T. Terencio, M. Srnec, M. Costas, J. Roithová, *J. Am. Chem. Soc.* **2017**, *139*, 2757–2765.

[11] L. S. Kau, D. J. Spira-Solomon, J. E. Penner-Hahn, K. O. Hodgson, E. I. Solomon, *J. Am. Chem. Soc.* **1987**, *109*, 6433–6442.

[12] J. Mehara, J. Roithová, *Chem. Sci.* **2020**, *11*, 11960–11972.

[13] G. L. Tripodi, M. M. J. Dekker, J. Roithová, L. Que, Jr., *Angew. Chem. Int. Ed.* **2021**, *60*, 7126–7131; *Angew. Chem.* **2021**, *133*, 7202–7207.

[14] a) K. Ray, F. Heims, M. Schwalbe, W. Nam, *Curr. Opin. Chem. Biol.* **2015**, *25*, 159–171; b) Z. Chen, D. Higgins, A. Yu, L. Zhang, J. Zhang, *Energy Environ. Sci.* **2011**, *4*, 3167–3192.

[15] The formation of hydrogen peroxide was excluded as its presence could neither be probed by iodometric titration nor by reaction with titanium oxysulfate. $H_2O_2$ is also found to be stable against disproportionation under catalytic turnover conditions (see Figure S20).